Beam Selection-Based Hybrid Precoding

Mariam Mussbah, Stefan Schwarz, and Markus Rupp
Institute of Telecommunications, Technische Universität Wien, Vienna, Austria
Christian Doppler Laboratory for Dependable Wireless Connectivity for the Society in Motion
Email: {mariam.mussbah, stefan.schwarz, markus.rupp}@tuwien.ac.at

***Abstract*—The deployment of large antenna arrays at the base station is a prerequisite for operating at the millimeter wave bands. The large antenna arrays are required to achieve high beamforming gains and thus to guarantee sufficient received signal power. In massive multiple input multiple output systems hybrid precoding is utilized to reduce power consumption and cost. Conventional precoder schemes require full channel knowledge at the transmitter, which is hard to obtain, especially in frequency division duplex systems. In this paper, we propose a novel hybrid precoding scheme, which requires only the information acquired during the initial access phase. Furthermore, we derive an analytical expression for characterizing the beam detection capabilities of the system.**

***Index Terms*—Beam management, hybrid precoding, massive MIMO, ROC.**

I. Introduction

Millimeter wave (mmWave) communication is a promising technology for the fifth generation (5G) of mobile communications and beyond [1]. To overcome the severe free space path loss at mmWave frequencies and maintain a sufficient link quality, directional beamforming is required. Due to the short wave length at high frequencies, many antennas can be packed into small form factors, making it possible to deploy massive multiple input multiple output (MIMO) systems and thus achieve high precoding gains [2]. For fully-digital beamforming the precoding is performed at the baseband and requires a radio frequency (RF) per antenna. Due to the high cost and high power consumption, traditional full digital beamforming is not suitable for massive MIMO. In order to overcome these issues, hybrid precoding has been proposed where the precoder is divided into two stages: an analog precoder and a low dimensional digital precoder [3], [4]. The author in [5], introduced low-resolution analog to digital converters, which allow to operate one RF chain per antenna as they become very cheap.

Several hybrid systems were proposed as solutions which strikes a balance between hardware complexity and system performance [6]–[12]. The authors in [6] consider a single user system and the authors in [7]–[10] consider a multi-user system. However, all aforementioned approaches require either the full channel state information (CSI) or the channel covariance matrix, which is not feasible for mmWave massive MIMO systems. Acquiring full CSI at the transmitter is hard since the hybrid structure prevents the channel estimation from directly accessing each antenna output, and due to the low signal to noise ratio (SNR) for non-precoded pilots. Furthermore, vehicular communication systems have a small channel coherence time, and thus require fast CSI acquisition and low complexity beamforming schemes. The authors in [11] propose a limited feedback hybrid precoding scheme but assume a single path channel model. In [12] the authors propose an angular-based user grouping algorithm to reduce the required CSI. In the first stage the authors design the analog precoder based on the angles of departure (AoD), and in the second stage the digital precoder is designed based on the effective channel which requires an additional step for acquiring CSI.

During the initial access phase neither at the base station (BS) nor at the user equipment (UE) CSI is available. Due to the relatively narrow beams the BS can only cover a limited area. 5G New Radio release 16 specifies a set of procedures for establishing a connection during the initial access phase. In 3rd Generation Partnership Project (3GPP) beam management is defined as a set of procedures to acquire and maintain a set of beams for a quality connection. According to [13] beam management includes at least the following aspects: beam sweeping, beam measurement, beam determination and beam reporting. In this paper we prose a hybrid precoding scheme based on the information acquired during the initial access phase. Furthermore, we characterize the beam detection capabilities of the system by deriving an analytical expression for the receiver operating characteristic (ROC) curve.

The following notation is used throughout this paper: $\mathbf{A}$ is a matrix, $\mathbf{a}$ is a vector, a is a scalar and the i-th column of $\mathbf{A}$ is denoted by $\mathbf{a}_i$. $\mathbf{1}$ denotes an all-ones vector. The transpose of a matrix is $\mathbf{A}^T$, the conjugate is $\mathbf{A}^H$ and the Frobenius norm is $\|\mathbf{A}\|_F$.

II. System Model

A. Signal Model

We consider an orthogonal frequency-division multiplexing (OFDM) multi-user mmWave transmission system in which the BS is equipped with N_t antennas and communicates with U UEs, each equipped with one RF chain and N_r antennas. Further, to enable multi-user communications we assume that the BS is equipped with N_t^{RF} RF chains such that $U \leq N_t^{\mathrm{RF}} \leq N_t$.

On the downlink the BS first precodes U data symbols at each subcarrier $k = 1, ..., K$ using a $N_t^{\mathrm{RF}} \times U$ baseband precoder $\mathbf{F}_{\mathrm{BB},k}$ followed by a $N_t \times N_t^{\mathrm{RF}}$ wideband RF precoder $\mathbf{F}_{\mathrm{RF}}$. Therefore, the discrete-time transmitted signal at subcarrier k is given by $\mathbf{x}_k = \mathbf{F}_{\mathrm{RF}}\mathbf{F}_{\mathrm{BB},k}\mathbf{s}_k$ where $\mathbf{s}_k \in \mathbb{C}^{U\times 1}$ denotes the signal vector of all UEs at subcarrier

k. Since the RF precoder is implemented using analog phase shifters and combiners, each element of $\mathbf{F}_{\text{RF}}$ is normalized to satisfy $|f_{\text{RF},i,j}| = \frac{1}{\sqrt{N_t}}$. The total transmit power constraint is enforced by normalizing $\mathbf{F}_{\text{BB}}$ to satisfy $\|\mathbf{F}_{\text{RF}}\mathbf{F}_{\text{BB}}\|_{\text{F}} = 1$. For an OFDM system with a sufficiently long cyclic prefix the signal received at UE u and subcarrier k can be expressed as

$$y_{u,k} = \mathbf{h}_{u,k}^H \mathbf{x}_k + n_{u,k}, \tag{1}$$

where the noise $n_{u,k}$ is assumed to be independent and identically distributed (i.i.d.) circularly symmetric Gaussian $\mathcal{CN}(0, \sigma_n^2)$.

B. Channel Model

Due to the sparse scattering nature of the mmWave channel [14] a geometric model with N_l scatterers is adopted. Furthermore, we assume that each scatterer contributes a single propagation path between BS and UE [15]. The channel associated with the u-th UE is given by [16]

$$\mathbf{h}_{u,k} = \sum_{l=1}^{N_l} \beta_{u,l} \mathbf{a}_t \left(\theta_l^{(t,u)}\right) \exp\left(-j2\pi f_k \tau_{u,l}\right) \tag{2}$$

where f_k denotes the frequency at the k-th subcarrier, $\tau_{u,l}$ denotes the delay, $\theta_l^{(t,u)}$ denotes the AoD. The complex path gain $\beta_{u,l}$ is Gaussian distributed $\beta_{u,l} \sim \mathcal{CN}(0, \sigma_{\beta_{u,l}}^2)$. $\mathbf{a}_r(\theta_l^{(r,u)})$ and $\mathbf{a}_t^T(\theta_l^{(t,u)})$ are the antenna array response vectors of the u-th UE and the BS, respectively. Given a uniform linear array (ULA) with N_t antennas the array steering vector is given by

$$\mathbf{a}_t(\theta_t) = \frac{1}{\sqrt{N_t}}(1, e^{j\frac{2\pi}{\lambda}d\cos(\theta_t)}, ..., e^{j\frac{2\pi}{\lambda}d\cos(\theta_t)(N_t-1)}), \tag{3}$$

with d denoting the inter-antenna spacing and λ denoting the wavelength.

III. Beam Detection

A. Beam Sweeping

In the beam sweeping phase the BS broadcasts a burst of synchronisation signal blocks (SSBs) each associated with a different beam. In 5G new radio (NR) each SSB occupies 240 consecutive subcarriers and four OFDM symbols. It contains four signals: primary synchronisation signal, secondary synchronisation signal, physical broadcast channel (PBCH) and the PBCH demodulation reference signal (PBCH-DMRS). Due to the absence of CSI in the initial access phase, precoding of the SSB burst, in time-varying directions so that each SSB is associated with a different beam which points in a different direction, is required.

In this paper we employ a codebook based beamforming strategy. The sparse scattering nature of mmWave transmissions results in a spatially correlated channel. Therefore, a discrete Fourier transform (DFT)-based codebook, which is suited for strongly correlated channels, is employed [17]. The DFT matrix $\mathbf{U}$ is a $N_t \times N_t$ unitary matrix whose elements are given by

$$u_{m,n} = \frac{1}{\sqrt{N_t}} e^{\frac{j2\pi(m-1)(n-1)}{N_t}} \tag{4}$$

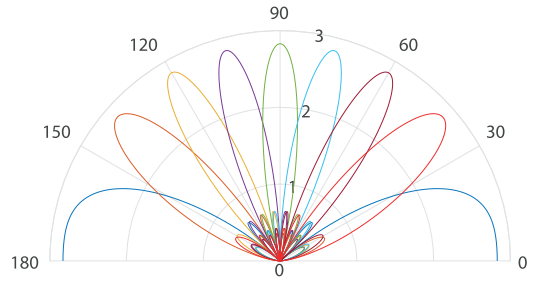

Fig. 1: Beamforming pattern of the DFT-based codebook for a ULA.

Each column of the DFT matrix corresponds to an analog precoder and all columns together form an orthonormal basis for $\mathbb{C}^{N_t}$. The DFT beamforming pattern for a ULA is shown in Fig. 1, where each color corresponds to a different column of $\mathbf{U}$. As Fig. 1 indicates, the DFT-based codebook allows sampling the angular domain and represents the channel in terms of these new input output coordinates [18]. The angular domain representation $\mathbf{h}_a \in \mathbb{C}^{N_t \times 1}$ of the channel $\mathbf{h} \in \mathbb{C}^{N_t \times 1}$ is given by $\mathbf{h}_a = \mathbf{U}\mathbf{h}$, where the i-th component of $\mathbf{h}_a$ is the aggregation of all paths whose direction fall within the i-th beam. Due to the sparsity assumption of the channel model, the angular domain representation $\mathbf{h}_a$ will be approximately sparse.

B. Beam Measurement and Determination

For each beamformed SSB the UE has to measure the signal strength and based on that, it has to determine whether there exits a path or not. The signal received by the UE can be expressed as

$$y_{k,u} = \mathbf{h}_{u,k}^H \mathbf{u}_i p_k + n_{k,u} \tag{5}$$

where p_k denotes a 4-QAM pilot symbol. By stacking the values of (5) over all subcarriers we obtain the received signal vector $\mathbf{y}_u$. The UE estimates the power by

$$P = \frac{1}{K} \|\mathbf{y}_u\|_2^2, \tag{6}$$

and compares it to a certain threshold γ, if the power is larger than this threshold, i.e., $P > \gamma$, a path is detected otherwise the UE assumes it just measured noise.

Determining the threshold is no trivial task. To evaluate the impact of the threshold on the classification accuracy a ROC analysis is required. The ROC curve plots the detection probability over the false alarm probability. The detection probability is given by the probability that P is larger than the threshold under the hypotheses that there is a single path between BS and UE, which will be denoted by $\mathcal{H}_1$, whereas the false alarm probability is given by the probability that P is larger than the threshold under the hypotheses that there is no path between BS and UE. Therefore, the distribution of the estimated power under both hypotheses is required. In what follows we will derive the distribution of P for both hypotheses, i.e., $f(P|\mathcal{H}_0)$ and $f(P|\mathcal{H}_1)$.

Under the assumption that $\mathcal{H}_0$ is true, $P = \sum_{k=1}^{K} |n_{k,u}|^2$. Since the noise is assumed to be circularly symmetric Gaus-

sian, the power P follows a chi-squared distribution with $2K$ degrees of freedom. Now let us that $\mathcal{H}_1$ is true and that the precoding $\mathbf{u}_i$ points into the direction of the l-th path, the received signal is given by

$$y_{u,k} = \beta_{u,l} e^{-j2\pi f_k \tau_i} p_k \mathbf{a}_t^H(\theta_{t,l})\mathbf{u}_i + \sum_{m \neq l} \beta_{u,m} e^{-j2\pi f_k \tau_m} \tilde{p}_k \mathbf{a}_t^H(\theta_{t,m})\mathbf{u}_i + n_{u,k}, \quad (7)$$

Since for large N_t the contribution from the side lobes is small compared to the main lobe, the second term in (8) is small and thus we treat it as noise $\tilde{n}_{u,k}$. Since the pilots are from a 4-QAM constellation, they can be expressed as $p_k = e^{j\phi_k}$ and (8) can be written as

$$y_{u,k} = \tilde{\beta}_{u,l}\tilde{p}_k + \tilde{n}_{u,k} \quad (8)$$

where $\tilde{\beta}_{u,l} = \beta_{u,l} \left|\mathbf{a}_t^H(\theta_{t,l})\mathbf{u}_i\right|$ and $\tilde{p}_k = e^{-j(2\pi f_k \tau - \phi_k - \arg(\mathbf{a}_t^H(\theta_{t,l})\mathbf{u}_i))}$. Since the $\tilde{n}_{u,k}$ and $\tilde{\beta}_{u,l}$ are both assumed to be circularly symmetric, the phase shift introduced by $\tilde{p}_k$ has no impact on the sum in (6). Therefore, we can rewrite the received signal as

$$\mathbf{y}_u = \tilde{\beta}_{u,l}\mathbf{1} + \tilde{\mathbf{n}}_u. \quad (9)$$

Below, we drop the subscript u and l for notational convenience, and write $\mathbf{y}_u$, $\tilde{\beta}_{u,l}$ and $\tilde{\mathbf{n}}_u$ as $\mathbf{y}$, β and $\mathbf{n}$, i.e.,

$$\mathbf{y} = \beta\mathbf{1} + \mathbf{n}. \quad (10)$$

Since the sum of Gaussian random variables is again Gaussian, and by computing the conditional mean vector and conditional covariance matrix, we find that the real and imaginary part of $\mathbf{y}$ follow a Gaussian distribution $\mathcal{CN}(\mathbf{0}, \mathbf{C}_y)$ where $\mathbf{C}_y = \sigma_n^2\mathbf{I} + \sigma_\beta^2\mathbf{1}\mathbf{1}^\mathbf{T}$.

Now the task is to find the distribution of $\mathbf{y}^H\mathbf{y} = \mathbf{y}_R^H\mathbf{I}\mathbf{y}_R + \mathbf{y}_I^H\mathbf{I}\mathbf{y}_I$. The real part $\mathbf{y}_R$ and the imaginary part $\mathbf{y}_I$ are uncorrelated and have the same correlation matrix $\frac{1}{2}\mathbf{C}_y$. According to [19], the quadratic form of the correlated random vector can be transformed to a quadratic form of an uncorrelated vector.

First let us introduce a new random variable

$$\tilde{\mathbf{y}}_\mathrm{R} = \mathbf{C}_y^{-\frac{1}{2}}\mathbf{y}_\mathrm{R}, \quad (11)$$

where the new vector $\tilde{\mathbf{y}}_\mathbf{R}$ is uncorrelated. The quadratic form can be rewritten as:

$$\begin{aligned}\mathbf{y}_R^H\mathbf{I}\mathbf{y}_\mathrm{R} &= \tilde{\mathbf{y}}_\mathrm{R}^H\mathbf{C}_y\tilde{\mathbf{y}}_\mathrm{R} \\ &= \tilde{\mathbf{y}}_\mathrm{R}^H\mathbf{V}^H\mathbf{\Lambda}\mathbf{V}\tilde{\mathbf{y}}_\mathrm{R} \\ &= \mathbf{z}_\mathrm{R}^H\mathbf{\Lambda}\mathbf{z}_\mathrm{R}\end{aligned}$$

where $\mathbf{V}$ and $\mathbf{\Lambda}$ are the eigenvector matrix and eigenvalue matrix of $\mathbf{C}_y$ and $\mathbf{z}_R = \mathbf{V}\tilde{\mathbf{y}}_\mathbf{R}$. Now the original problem can be rewritten as

$$\mathbf{y}^H\mathbf{y} = \sum_{k=1}^{K} \lambda_k z_{\mathrm{R},k}^2 + \sum_{k=1}^{K} \lambda_k z_{\mathrm{I},k}^2 \quad (12)$$

where the eigenvalues λ_k of the correlation matrix $\mathbf{C}_y$ are given by

$$\lambda_k = \begin{cases} \sigma_n^2 & 1 \leq k < K \\ \sigma_n^2 + \sigma_\beta^2 K & k = K \end{cases} \quad (13)$$

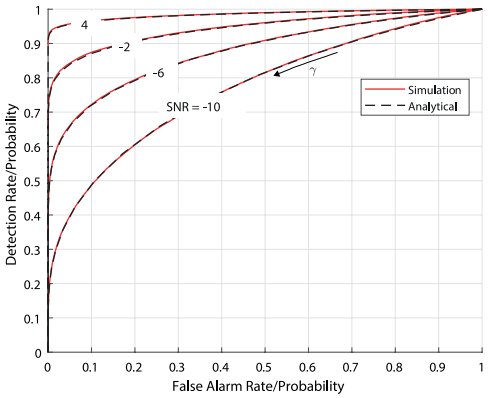

Fig. 2: The ROC for different SNR values.

Since the vectors $\mathbf{z}_\mathrm{R}$ and $\mathbf{z}_\mathrm{I}$ are i.i.d. Gaussian with zero mean and unit variance, the sum can be rewritten as

$$\mathbf{y}^H\mathbf{y} = \sigma_k^2 \sum_{k=1}^{K-1} (z_{\mathrm{R},k}^2 + z_{\mathrm{I},k}^2) + (\sigma_k^2 + \sigma_\beta^2 K)(z_{\mathrm{R},K}^2 + z_{\mathrm{I},K}^2). \quad (14)$$

The first term in (14) is a sum of $2(K-1)$ i.i.d. random variables and according to the central limit theorem the distribution of the sum can be approximated by a Gaussian distribution with mean $\mu_1 = 2\sigma_n^2\frac{(K-1)}{K}$ and variance $\sigma_1^2 = 4\sigma_n^4\frac{(K-1)}{K^2}$. The second term in (14) follows an exponential distribution with mean $\mu_2 = 2\frac{\sigma_n^2 + K\sigma_\beta^2}{K}$. The sum of the two terms results in an exponentially modified Gaussian distribution [20] and the corresponding distribution function is

$$f(P;\mu_1,\sigma_1,\mu_2) = \frac{\mu_2}{2}\exp\left(\frac{\mu_2}{2}(2\mu_1 + \mu_2\sigma_1^2 - 2P)\right) \times \operatorname{erfc}\left(\frac{\mu_1 - \mu_2\sigma_1^2 - P}{\sqrt{2}\sigma_1}\right), \quad (15)$$

and thus the detection probability P_D can now be calculated by

$$P_D = \int_\gamma^\infty f(P;\mu_1,\sigma_1,\mu_2|\mathcal{H}_1)\mathrm{dP}. \quad (16)$$

Fig. 2 shows that the analytical ROC and the ROC obtained via simulation match very well. The ROC curves show the detection/false alarm probability trade-off for all possible thresholds, thus allowing the selection of a threshold according to specific requirements.

C. Beam Reporting

In order for the UE to report the selected beams, it has to wait for the BS to schedule a random access channel towards the direction of detected beams. Based on the reported beams the BS has to select a set of beams to establish a connection to all UEs in the cell.

IV. Beam Selection Based Hybrid Precoding

The objective is to design hybrid precoding matrices based on the reported beams, so that the achievable sum rate is maximized. At the BS we assume that the detected beams for each UE are known. Furthermore, we assume that the effective channel, i.e.,

$$\mathbf{h}_{u,k,\mathrm{eff}} = \tilde{\mathbf{U}}\mathbf{h}_{u,k}, \quad (17)$$

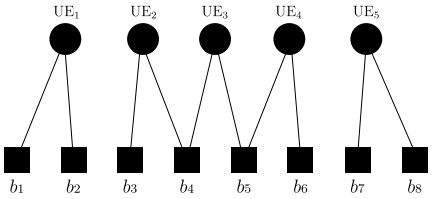

Fig. 3: An example of the grouping stage. The circles represent the UEs, the squares represent the beams and the edges indicate the reported beams.

where the columns of $\tilde{\mathbf{U}}$ are given by the columns of the DFT matrix for which a beam was detected. Thus $\mathbf{h}_{u,k,\text{eff}}$ is the projection of the channel in the space spanned by the reported beams, is known.

According to the model of the received signal given in (1), the achievable rate of the u-th UE is

$$R_u = \sum_{k=1}^{K} \log_2 \left(1 + \frac{\left| \mathbf{h}_{u,k}^H \mathbf{F}_{\text{RF}} \mathbf{f}_{\text{BB},k,u} \right|^2}{\sum_{i \neq u} \left| \mathbf{h}_{u,k}^H \mathbf{F}_{\text{RF}} \mathbf{f}_{\text{BB},k,i} \right|^2 + \sigma_n^2} \right), \quad (18)$$

and the sum rate of the system is

$$R = \sum_{u=1}^{U} R_u \quad (19)$$

We propose a hybrid precoding scheme that consists of two stages, namely, the grouping stage and the beam selection stage.

A. Grouping

In the grouping stage the UEs are divided into groups so that UEs, who have reported the same beams are in one group. The grouping stage will be explained, based on the example shown in Fig. 3, which consists of 5 UEs and 8 beams. UE_1 has reported beam index b_1 and b_2 and since no other UE has reported these indices the first group consists only of one UE, i.e., $\mathcal{G}_1 = \{\text{UE}_1\}$. Since UE_2 and UE_3 reported beam index b_4 and UE_3, UE_4 reported b_5, the second group is given by $\mathcal{G}_2 = \{\text{UE}_2, \text{UE}_3, \text{UE}_4\}$. Lastly, similar to $\mathcal{G}_1$ we have $\mathcal{G}_3 = \{\text{UE}_5\}$. As indicated in Fig. 3, the grouping problem is equivalent to partitioning the graph into connected components for which efficient algorithms exists [21].

B. Best Precoder Selection

In the precoder selection stage, the BS selects the analog precoder based on the beams reported. In the digital domain we adopt a zero forcing (ZF) precoder, which is calculated based on the effective channel. Since the groups are approximately orthogonal, i.e., UEs in different groups do not have common beams reported, the precoder for each group can be determined independently of the other groups. The analog precoder is given by

$$\mathbf{F}_{\text{RF}} = \begin{bmatrix} \mathbf{F}_{\text{RF}}^{(1)} & \dots & \mathbf{F}_{\text{RF}}^{(G)} \end{bmatrix}, \quad (20)$$

where $\mathbf{F}_{\text{RF}}^{(g)}$ denotes the analog precoder of the g-th group and G denotes the number of groups. The digital precoder is given by

$$\mathbf{F}_{\text{BB}} = \begin{bmatrix} \mathbf{F}_{\text{BB}}^{(1)} & \mathbf{0} & \cdots & \mathbf{0} \\ \mathbf{0} & \mathbf{F}_{\text{BB}}^{(2)} & \cdots & \mathbf{0} \\ \vdots & \vdots & \ddots & \vdots \\ \mathbf{0} & \mathbf{0} & \cdots & \mathbf{F}_{\text{BB}}^{(G)} \end{bmatrix}, \quad (21)$$

where $\mathbf{F}_{\text{BB}}^{(g)}$ denotes the digital precoder of the g-th group and is of size $K_g \times K_g$ with K_g denoting the size of group g.

The groups are further divided into two categories: single user and multi-user. Groups which consist of only one user belong to the single user category and all other groups belong to the multi-user category.

1) Single User Precoding

UEs which belong to the single user category have reported unique beams, i.e., they do not have common beams with any other UEs in the cell. Therefore, the beam index can be directly selected as the beam that results in the highest power. If we assume that for the example given above that the reported estimated power for beam b_1 is higher than the power reported for beam b_2, then the analog precoder for $\mathcal{G}_1$ is given by

$$f_{\text{RF}}^{(1)} = \mathbf{u}_{b_1}, \quad (22)$$

where $\mathbf{u}_{b_1}$ denotes the b_1-th column of the DFT matrix. Furthermore, since the group consists of only one UE, the digital precoder becomes a scalar and is given by

$$f_{\text{BB}}^{(1)} = \frac{1}{\sqrt{K}} \quad (23)$$

2) Multi-User Precoding

For the multi-user groups an exhaustive search among all possible analog precoders is performed to find the best beam indices. Let $\mathbf{F}_{\text{RF},c}^{(g)}$ denote the $N_t \times K_g$ analog precoder of the c-th combination of beams. The combined channel of the group is given by vertically stacking the channels of all UEs in the group. For the example shown in Fig. 3, the combined channel of $\mathcal{G}_2$ is given

$$\mathbf{H}_k^{(2)} = \begin{bmatrix} \mathbf{h}_{2,k} & \mathbf{h}_{3,k} & \mathbf{h}_{4,k} \end{bmatrix}^H, \quad (24)$$

and the effective channel is given by $\tilde{\mathbf{H}}_k^{(2)} = \mathbf{H}_k^{(2)} \mathbf{F}_{\text{RF},c}^{(2)}$. Given the effective channel, the ZF digital precoder is given by

$$\mathbf{F}_{\text{BB},c}^{(2)} = \alpha \tilde{\mathbf{H}}_k^{(2)H} \left(\tilde{\mathbf{H}}_k^{(2)} \tilde{\mathbf{H}}_k^{(2)H} \right)^{-1}, \quad (25)$$

where $\alpha = \sqrt{\frac{K_g}{K}} \left\| \tilde{\mathbf{H}}_k^{(2)H} (\tilde{\mathbf{H}}_k^{(2)} \tilde{\mathbf{H}}_k^{(2)H})^{-1} \right\|_F^{-2}$ is the normalization factor.

The precoders for the g-th group are given by

$$\mathbf{F}_{\text{BB}}^{(g)}, \mathbf{F}_{\text{RF}}^{(g)} = \underset{\mathbf{F}_{\text{BB},c}^{(g)}, \mathbf{F}_{\text{RF},c}^{(g)}}{\arg\max} R^{(g)}, \quad (26)$$

where $R^{(g)} = \sum_{u \in \mathcal{G}_g} R_u$.

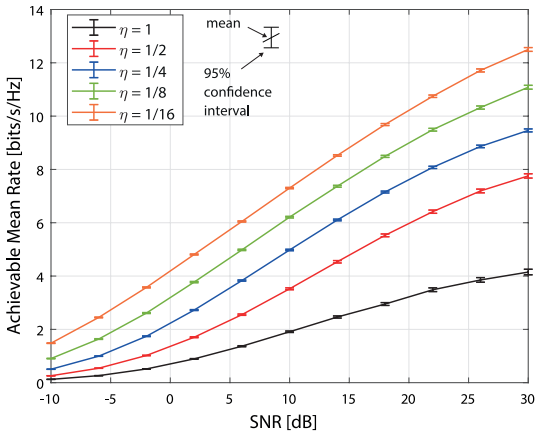

Fig. 4: Average sum rate as a function of the SNR for different number of users to number of antennas ratio.

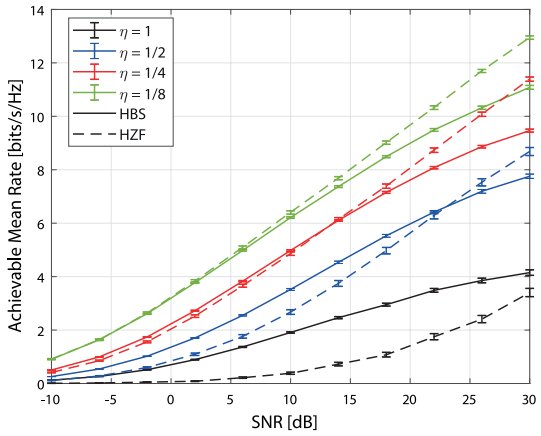

Fig. 5: Average sum rate for the proposed hybrid beam selection scheme and the hybrid ZF as a function of the SNR.

V. Numerical Results

In this section, we evaluate the performance of our proposed precoding scheme by running Monte-Carlo simulations. The performance of the proposed scheme is shown in terms of an achievable mean sum rate. In our simulation we consider a BS equipped with a ULA consisting of N_t isotropic antennas. The spacing between the antenna elements is half-wavelength. The UEs are equipped with one antenna each. The channel between a BS and a UE has four paths, the mean power of each path is generated according to a PedestrianA power delay profile. The angles of arrivals (AoAs) and AoDs for every path are distributed according to $\mathcal{U}(0, \pi)$.

The simulation results are shown in Fig. 4, where each curve corresponds to a different ratio of $\eta = U/N_t$. As expected, the performance increases as the ratio η decrease. Since the received power is proportional to the number of antennas, we can see that for $\eta < 0.25$ doubling the number antennas compared to the number of UEs, results in a 3dB shift. Thus, for small values of η the increase of performance is due to the increased power. Whereas, for $\eta > 0.25$ we observe a larger shift between the curves, which is due to the fact that for large η the interference is still large and decreasing the ratio leads to a better interference suppression. Furthermore, due to the limited beam detection capabilities we observe a saturation of the rate at high SNR.

In Fig. 5 we compare our proposed hybrid beam selection scheme to the hybrid ZF scheme proposed in [22]. We can see that for noise limited systems our proposed scheme outperforms the hybrid ZF. Since the hybrid ZF scheme assumes the full channel knowledge at the BS, it outperforms the proposed scheme for interference limited system.

VI. Conclusions

In this paper, we proposed a low complexity hybrid precoding scheme, where we utilize the CSI acquired during the initial access. Based on the reported beam, we divide the UEs into groups and design the analog precoder to eliminate the inter-group interference an to maximize the achievable rate. In the second stage we eliminate the intra-group interference by applying a ZF precoder at baseband. We analyzed the performance of the proposed scheme assuming a sparse channel model with four paths. We observe that for noise limited systems, our proposed scheme outperforms the hybrid ZF, which requires full CSI. Whereas for high SNR the hybrid ZF achieves better performance due to the limited detection capabilities of the system. Furthermore, we provided an analytical characterization of the beam detection capabilities of the system.

Acknowledgements

The financial support by the Austrian Federal Ministry for Digital and Economic Affairs and the National Foundation for Research, Technology and Development is gratefully acknowledged.

References

[1] R. W. Heath, N. González-Prelcic, S. Rangan, W. Roh, and A. M. Sayeed, "An Overview of Signal Processing Techniques for Millimeter Wave MIMO Systems," *IEEE Journal of Selected Topics in Signal Processing*, vol. 10, no. 3, pp. 436–453, 2016.

[2] F. Rusek, D. Persson, B. K. Lau, E. G. Larsson, T. L. Marzetta, O. Edfors, and F. Tufvesson, "Scaling Up MIMO: Opportunities and Challenges with Very Large Arrays," *IEEE Signal Processing Magazine*, vol. 30, no. 1, pp. 40–60, 2013.

[3] S. Han, C. I, Z. Xu, and C. Rowell, "Large-scale antenna systems with hybrid analog and digital beamforming for millimeter wave 5G," *IEEE Communications Magazine*, vol. 53, no. 1, pp. 186–194, 2015.

[4] J. A. Zhang, X. Huang, V. Dyadyuk, and Y. J. Guo, "Massive hybrid antenna array for millimeter-wave cellular communications," *IEEE Wireless Communications*, vol. 22, no. 1, pp. 79–87, 2015.

[5] L. N. Ribeiro, S. Schwarz, M. Rupp, and A. L. F. de Almeida, "Energy Efficiency of mmWave Massive MIMO Precoding With Low-Resolution DACs," *IEEE Journal of Selected Topics in Signal Processing*, vol. 12, no. 2, pp. 298–312, 2018.

[6] O. E. Ayach, S. Rajagopal, S. Abu-Surra, Z. Pi, and R. W. Heath, "Spatially Sparse Precoding in Millimeter Wave MIMO Systems," *IEEE Transactions on Wireless Communications*, vol. 13, no. 3, pp. 1499–1513, 2014.

[7] J. Cai, B. Rong, and S. Sun, "A Low Complexity Hybrid Precoding Scheme for Massive MIMO System," in *2016 16th International Symposium on Communications and Information Technologies (ISCIT)*, 2016, pp. 638–641.

[8] L. Liang, W. Xu, and X. Dong, "Low-Complexity Hybrid Precoding in Massive Multiuser MIMO Systems," *IEEE Wireless Communications Letters*, vol. 3, no. 6, pp. 653–656, 2014.

[9] Y. Huang, C. Liu, Y. Song, and X. Yu, "DFT Codebook-Based Hybrid Precoding for Multiuser mmWave Massive MIMO Systems," *EURASIP*

Journal on Applied Signal Processing, vol. 2020, no. 1, p. 11, Mar. 2020.

[10] W. Ni and X. Dong, "Hybrid Block Diagonalization for Massive Multiuser MIMO Systems," *IEEE Transactions on Communications*, vol. 64, no. 1, pp. 201–211, 2016.

[11] A. Alkhateeb, G. Leus, and R. W. Heath, "Limited Feedback Hybrid Precoding for Multi-User Millimeter Wave Systems," *IEEE Transactions on Wireless Communications*, vol. 14, no. 11, pp. 6481–6494, 2015.

[12] A. Koc, A. Masmoudi, and T. Le-Ngoc, "3D Angular-Based Hybrid Precoding and User Grouping for Uniform Rectangular Arrays in Massive MU-MIMO Systems," *IEEE Access*, vol. 8, pp. 84 689–84 712, 2020.

[13] 3rd Generation Partnership Project (3GPP), "Technical Specification Group Radio Access Network; Study on New Radio Access Technology; Physical layer Aspects," 3rd Generation Partnership Project (3GPP), TR 38.802, Mar. 2017.

[14] M. R. Akdeniz, Y. Liu, M. K. Samimi, S. Sun, S. Rangan, T. S. Rappaport, and E. Erkip, "Millimeter Wave Channel Modeling and Cellular Capacity Evaluation," *IEEE Journal on Selected Areas in Communications*, vol. 32, no. 6, pp. 1164–1179, 2014.

[15] A. Alkhateeb, O. El Ayach, G. Leus, and R. W. Heath, "Channel Estimation and Hybrid Precoding for Millimeter Wave Cellular Systems," *IEEE Journal of Selected Topics in Signal Processing*, vol. 8, no. 5, pp. 831–846, 2014.

[16] R. Zhang, J. Zhang, T. Zhao, and H. Zhao, "Block Sparse Recovery for Wideband Channel Estimation in Hybrid mmWave MIMO Systems," in *2018 IEEE Global Communications Conference (GLOBECOM)*, 2018, pp. 1–6.

[17] Lei Wan, Xiaofeng Zhong, Yousi Zheng, and Shunliang Mei, "Adaptive codebook for limited feedback MIMO system," in *2009 IFIP International Conference on Wireless and Optical Communications Networks*, 2009, pp. 1–5.

[18] D. Tse and P. Viswanath, *Fundamentals of Wireless Communication*. Cambridge University Press, 2005.

[19] A. Mathai and S. Provost, *Quadratic Forms in Random Variables*, ser. Statistics: A Series of Textbooks and Monographs. Taylor & Francis, 1992. [Online]. Available: https://books.google.at/books?id=tFOqQgAACAAJ

[20] E. Grushka, "Characterization of Exponentially Eodified Gaussian Peaks in Chromatography," *Analytical chemistry*, vol. 44, no. 11, p. 1733—1738, September 1972. [Online]. Available: https://doi.org/10.1021/ac60319a011

[21] J. Hopcroft and R. Tarjan, "Algorithm 447: Efficient Algorithms for Graph Manipulation," *Commun. ACM*, vol. 16, no. 6, p. 372–378, Jun. 1973. [Online]. Available: https://doi.org/10.1145/362248.362272

[22] L. Liang, W. Xu, and X. Dong, "Low-Complexity Hybrid Precoding in Massive Multiuser MIMO Systems," *IEEE Wireless Communications Letters*, vol. 3, no. 6, pp. 653–656, 2014.